SAFETY ANALYSIS OF THE REACTIVITY TRANSIENTS RESULTING FROM WATER INGRESS INTO A HIGH-TEMPERATURE PEBBLE BED REACTOR

RAHIM NABBI, WILFRIED JAHN, GERHARD MEISTER,
and WERNER REHM *Kernforschungsanlage Jülich*
Institut für Nukleare Sicherheitsforschung, Postfach 1913
D-5170 Jülich 1, Federal Republic of Germany

Received November 5, 1982
Accepted for Publication February 2, 1983

Analysis of extreme water ingress accidents in the pebble bed high-temperature reactor of 500-MW(thermal) power during the first few minutes shows that the temperature coefficients of reactivity limit the power increase, presupposing no action of the shutdown system and other safety devices. The rupture of all steam generator tubes with the highest ingress rate of 55 kg/s results in a power maximum of 1.8 times the initial value after ~1 min. The system pressure increases from the operating value of 40 bar up to the design value of 50 bar. Fuel temperatures do not reach values that cause fuel particle damage and fission product release. Hence, special requirements on the promptness of shutdown rod actions are not needed to limit accident consequences in the core. Overpressurization of the reactor vessel will arise, however, if water ingress with the highest rate continues. Water ingress at a small rate (7 kg/s), corresponding to the rupture of a few tubes, results in a rather slow power increase up to 1.3 times the initial value and to a primary system pressure of 43 bar after 5 min.

I. INTRODUCTION

Some concern has arisen in the past with regard to a possible water ingress into the primary circuit of a high-temperature reactor (HTR) while the reactor is operated at full power. Since the core of this reactor type normally has an undermoderated composition, a water or steam ingress would cause an increase of reactivity resulting in an inadvertant power increase. Since accidents of this type have to be intercepted by the release of the shutdown rod system, i.e., by an active safety system, the question arises in this case about the consequences to be expected if the shutdown system is not immediately available for any reason (for instance, due to a failure in the reactor protection system).

In order to answer this question, water ingress accidents have been analyzed on the supposition that the shutdown system will not be activated. This paper gives information on the relevance of the function of the shutdown system and on the requirements for its promptness.

Several investigations relating to the consequence of a water ingress have previously been published. The reactivity effect of water in typical core compositions as used in HTRs has been determined by steady-state reactivity evaluations.[1,2] Earlier investigations on the dynamic behavior of the reactor in case of water ingress from a defective steam generator have been presented in Refs. 3, 4, and 5.

The investigation presented in this paper is motivated by the experience that the neutron kinetics response of the reactor is sensitively dependent on the time behavior of the mass flow, the steam partial pressure, and the gas temperature at the core inlet.[6] The analysis, therefore, has been performed using methods that comprise a simulation of the transport of steam in the primary circuit following a water ingress from a defective steam generator.

The system underlying the study presented here is the PNP-500 power plant. This plant, designed for 500-MW(thermal) power, is one of the HTR concepts projected for the generation of process heat. The results of this study, however, are assumed to be typical of HTRs that have undermoderated core

compositions and comparable negative temperature coefficients of reactivity.

A short description of the plant is given here insofar as it is necessary to judge the results obtained. The simulation programs used to analyze the plant response are explained with regard to relevant modeling features.

II. PLANT DESCRIPTION

The designation PNP-500 is used for a projected power plant comprising an HTR that is designed to supply process heat for chemical processes such as coal gasification and hydrogasification. The hot gas temperature is in the range of 950°C and thus essentially higher than that of HTR plants designed for electricity generation only. The heat removal system also contains special components, such as steam reformers and coal gasification devices, which are required for the chemical process system.

Figure 1 schematically shows a part of the heat removal system. Two different heat removal loops are shown. The loop on the left comprises a steam reformer and a steam generator connected in series. This is a typical arrangement for the hydrogasification of lignite. The steam reformer generates hydrogen from methane, using part of the output of the steam generator. The rest of the loop contains additional components required for the hydrogasification process, which are not shown. A second loop of the heat removal system is planned as a system for hard coal gasification. In contrast to the hydrogasification loop, this type of loop is separated from the primary circuit of the reactor by an intermediate gas-gas heat exchanger. The detailed arrangement of components in this loop is not shown either because it is not relevant to the investigation presented here. Details are described in Ref. 7.

The core of the reactor and the main components of the heat removal system are contained in cavities of a pressure vessel made of prestressed concrete. The central cavity contains the core, consisting of a packed bed of fuel spheres and the graphite reflectors surrounding the core. Heat is removed from the core by the forced convection of helium.

The packed bed forming the reactor core has a cylindrical shape with a 5.6-m diam and a 5.08-m effective height. The average power density at nominal power is 4 MW/m^3. The spherical fuel elements have an 0.06-m o.d. They consist of an inner fuel-graphite matrix with a 0.05-m diam surrounded by a fuel-free graphite shell. The core contains ~670 000 fuel spheres. Each fuel sphere contains ~14 000 small fuel particles with a 0.9-mm diam. These fuel particles consist of a uranium oxide kernel surrounded by several layers of pyrolytic graphite including one layer consisting of silicon carbide ("coated particles" of Triso type). This coating acts as an effective barrier for fission products generated in the uranium kernel. Low-enrichment fuel will be used in the core of the PNP-500 plant. Two core

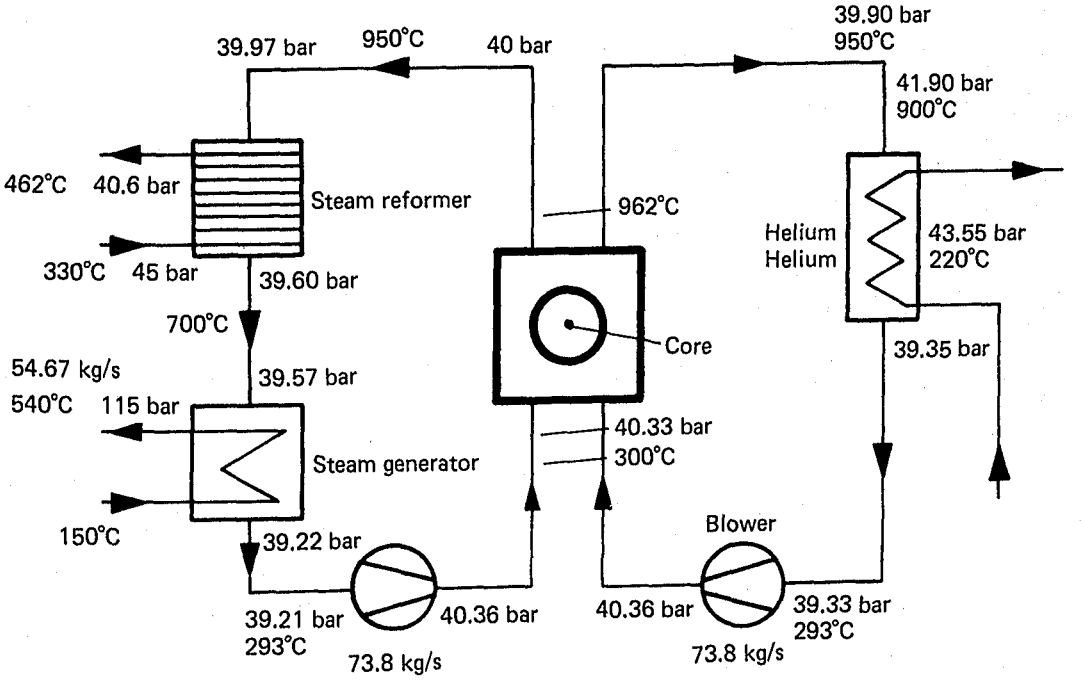

Fig. 1. Primary loop of the PNP-500 with steam reformer, steam generator, and helium-helium intermediate heat exchanger.

regions with different enrichment are taken into consideration. The (radially) outer region of the core will have an enrichment (12.6%) that is about two times larger than that in the central region (6.8%). The fuel spheres are continuously fed into the core at the top and withdrawn from the core at the bottom during operation of the reactor. Their average residence time in the core is ~4 yr. Withdrawn fuel spheres will not be reloaded ("once through, then out" = OTTO cycle). The axial power distribution in the core resulting from this type of refueling procedure has a distinct maximum in the upper part of the core.

The primary gas circuit is operated at a 40-bar pressure. Under normal operating conditions, the coolant is forced by blowers through the core in a downward direction. The gas mass flow is chosen so that a hot gas temperature of 950°C is attained with nominal power generation and with an inlet temperature of 303°C.

The heat is transported from the core to the heat exchanging components of the primary system via coaxial gas ducts as shown in Fig. 2. The cold gas returned to the core flows through channels in the side and top reflectors before entering the core. The different flow parts of the coolant are schematically shown in Fig. 3. The essential design data for the nuclear heat generation system are listed in Table I.

This investigation is concerned with the steam generator, which is operated in the hydrogasification loop in series with the steam reformer. This steam generator is considered to be of the helix bundle type in the present design. The secondary fluid flows through tubes that are arranged in bundles of 168 parallel tubes of equal length. They are connected to a common feeder at the inlet and to a common riser at the outlet of the secondary flow. The heat exchanging tubes have a 2.0-cm o.d. and a 0.23-mm wall thickness. The material is Incoloy 800. Each tube is 78.6 m long; the bundle height is 14 m. The total heat exchanger area on the primary side is 830 m^2.

Primary and secondary fluid flow take opposite directions. The secondary fluid flows in an upward direction so that "uphill boiling" prevails in the evaporation section.

The steam generator is designed in such a manner that the feedwater supply and the steam outlet junctions are arranged at the bottom of the system. The transferred power under normal operating conditions is 155 MW(thermal).

The reactor is equipped with a separate auxiliary

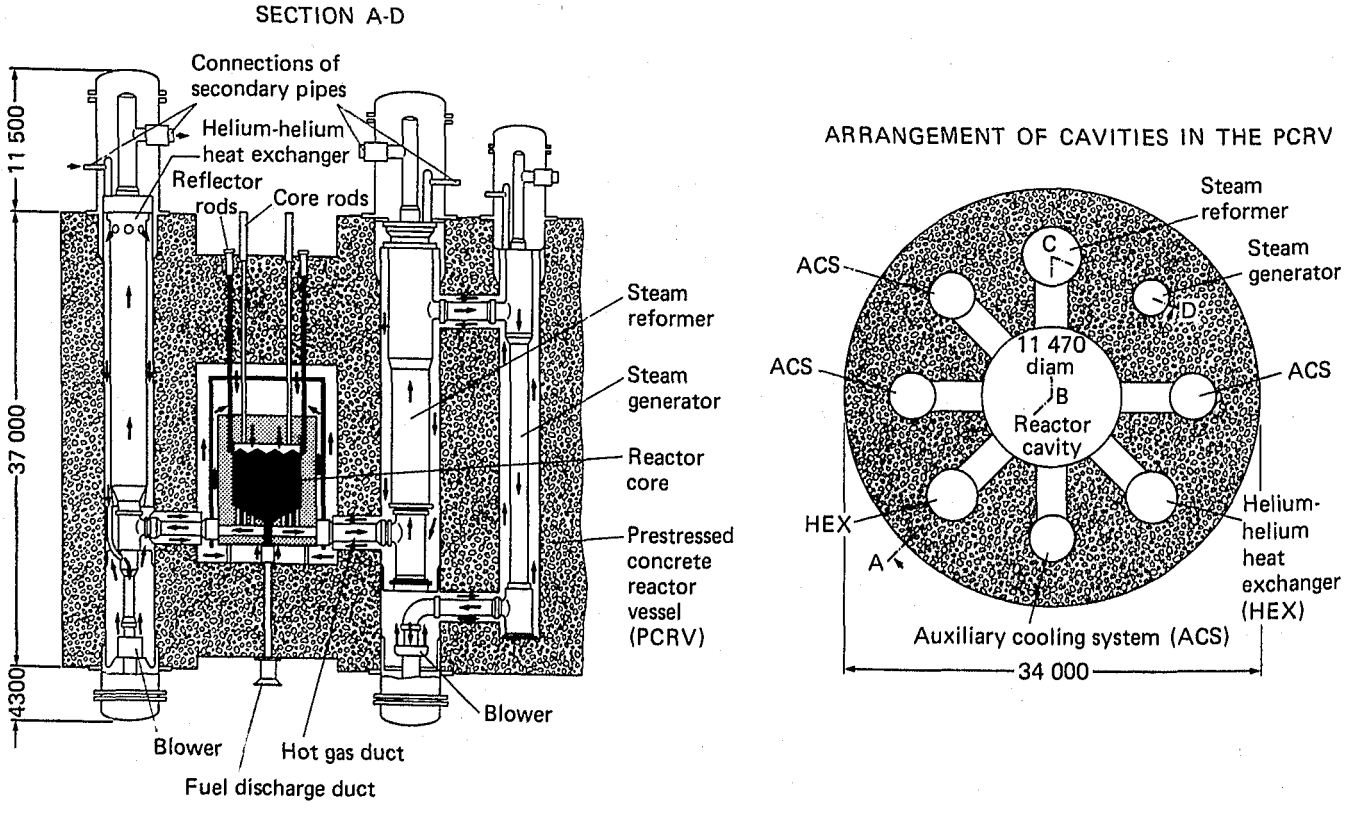

Fig. 2. Arrangement of the primary components in the pressure vessel.

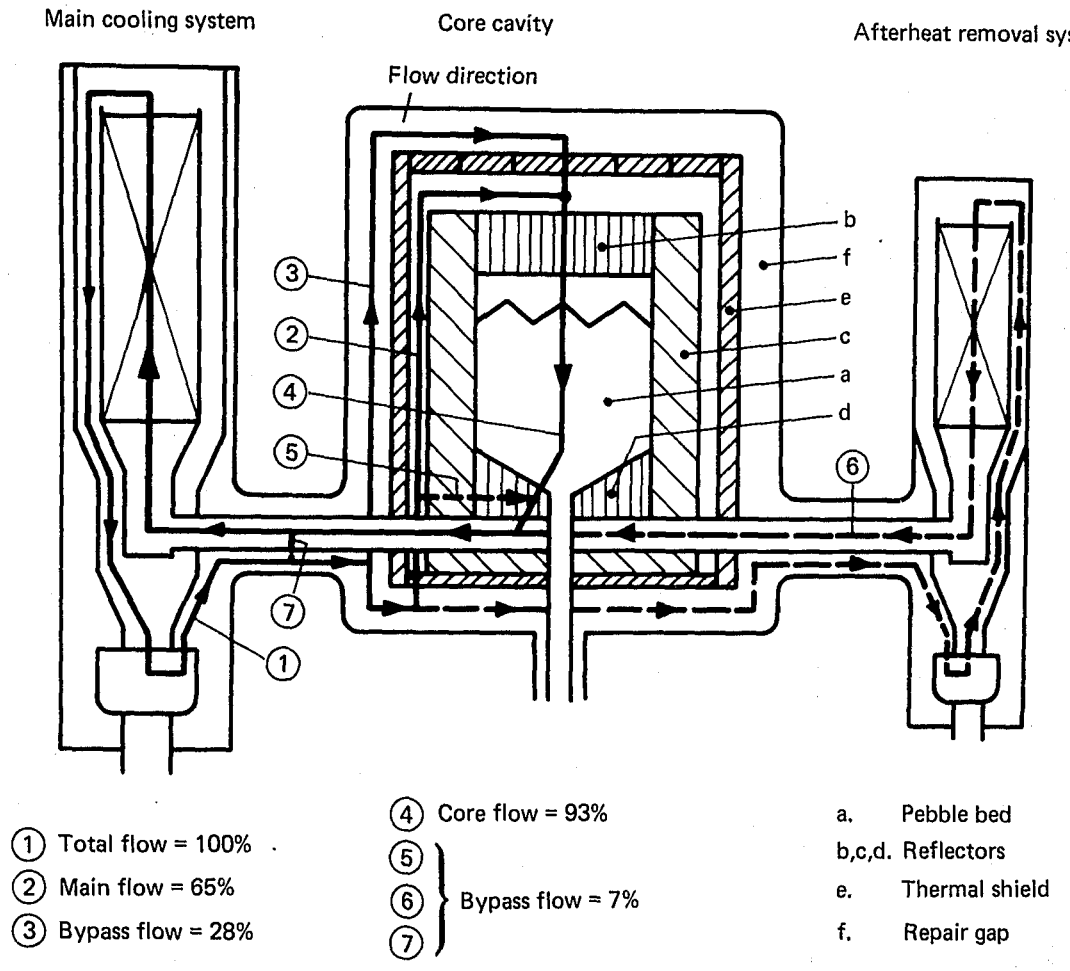

Fig. 3. Schematic pattern of the parts of the mass flow in the core cavity, the main cooling system, and the after-heat removal system.

system for the removal of decay heat after shutdown. This system comprises four independent loops coupled to the primary system by gas-gas heat exchangers. The heat is finally rejected to the surrounding coolers.

The plant has two systems of absorber rods that are available for reactor shutdown. The first system comprises 36 absorber rods located in vertical tubes in the side reflector. This system is intended for use as a rapid shutdown system only. It is activated by deenergizing magnetic coupling clutches. The rods will fall to their down position within 12 s. The shutdown reactivity held by this system amounts to about \$10.0.

The second system consists of 54 absorber rods that can be driven into the packed bed of the core. These rods are used for plant control but may also act as an additional shutdown system. In case of a rapid shutdown signal, these rods will be driven into the core over a 100-cm distance with a velocity of 2 cm/s. The additional shutdown reactivity available in this range depends on the initial position of the rods. On average, however, it will be about \$8.0. It can be made effective within 50 s. Additional reactivity absorption may be required during cooling down of the core as a consequence of reactivity gain resulting from the negative temperature coefficient of reactivity. This may be achieved from the latter system by driving the rods deeper into the core (up to 4.5 m).

A water ingress will be detected by the plant protection system through moisture detection devices in the primary system and, in the case of their failure, after some time by the resulting pressure and nuclear power increase. The moisture detection system generates a trip signal if the local steam concentration exceeds 500 vpm. In case of a water ingress, the plant protection system will initiate the following counteraction:

1. A rapid shutdown will be initiated by release of the shutdown absorber systems.

TABLE I

Main Design Data of the Nuclear Heat Generation System of the Nuclear Power Plant PNP-500 (Ref. 6)

Reactor	
Thermal power, MW	500
Average power density (core), MW/m^3	4
Helium mass flow, kg/s	145.0
Helium inlet/outlet temperature, °C	300/962
Helium inlet/outlet pressure, bar	40.3/40.0
Hydrogasification loop	
Helium mass flow, kg/s	73.8
Total pressure drop, bar	1.15
Steam reformer	
Helium inlet/outlet temperature, °C	950/700
Helium inlet/outlet pressure, bar	40.0/39.6
Feedgas inlet/outlet temperature at catalyst, °C	560/810
Feedgas inlet pressure at recuperator, bar	45.0
Feedgas outlet pressure at recuperator, bar	42.0
Steam generator	
Helium inlet/outlet temperature, °C	700/293
Helium inlet/outlet pressure, bar	39.6/39.2
Feedwater temperature, °C	150
Outlet steam temperature, °C	540
Outlet steam pressure, bar	115
Coal hydrogeneration loop	
Helium mass flow, kg/s	73.8
Total pressure loss, bar	1.03
Heat exchanger (helium/helium)	
Inlet/outlet temperature, °C	950/293
Inlet/outlet pressure, bar	39.9/39.4
Secondary inlet/outlet temperature, °C	220/900
Secondary inlet/outlet pressure, bar	43.6/41.9

2. The main heat removal system will undergo a controlled shutdown, and the auxiliary heat removal system will be started up.
3. The steam generator will be isolated from the primary system by closing slide valves in the primary flow path.
4. The steam ingress will be interrupted by shutting off the feedwater supply.

The delay time from the initiation of a water ingress to the complete isolation of the defective steam generator is mainly determined by two time spans. The first time interval is the time required to attain the steam concentration corresponding to the trip level of the moisture detectors. This time interval is mainly determined by the ingress rate. The second time interval is the time required for the isolation procedure. This latter time interval is assumed to be not much less than ~10 s.

In order to protect the reactor pressure vessel from damage by overpressurization, relief valves are provided that will cause a controlled blowdown if the pressure in the primary system exceeds a certain limit. It is assumed that it will not be much in excess of the design pressure of the 50-bar vessel.

III. ACCIDENT INITIATION, PRESUPPOSITIONS, AND INITIAL CONDITIONS

The initiating event for the accident being analyzed is a rupture of one or several heat exchanging tubes in the steam generator. The location of the rupture is assumed to be the steam superheating part where materials strains are expected to be highest. Since steam generators in HTRs are operated at a secondary pressure in a range above 125 bar and since the pressure in the primary circuit is 40 bar, a tube failure will result in a water ingress into the primary system. The blowers will force the steam-helium mixture through the reactor core and will gradually distribute the ingressed steam over the total primary circuit. Since the flow from the point of ingress to the core inlet is subject to many disturbances, which increase the turbulent mixing within the gas steam, it is assumed that the gas flow composition is radially homogeneous at the core inlet plane. To meet the objective of this investigation, the following assumptions about the behavior of the plant control and of the plant protection system will be made: No counteraction by active safety devices of the plant protection system will be available at least within the first time interval of ~1 min after initiation of the ingress. This includes the presupposition that the reactor will not be shut down by the absorber rods of the shutdown system and that the defective steam generator will not be isolated from the primary system. The automatic flow control system will be assumed to keep the volume flow rate of the gas blowers constant, irrespective of the instantaneous effective density of the steam-helium mixture. The gas outlet temperature of both heat removal loops will also be kept constant by the corresponding control system during the period of water ingress. This assumption is an acceptable approximation in view of the constant primary volume flow and if, in addition, the secondary flow rate and inlet temperature of the heat exchanging components are also assumed to be constant.

The increasing steam content in the primary circuit produces, besides the reactivity effects in the reactor core, an increase of pressure due to mass and energy inflow and causes graphite corrosion due to the chemical reactions between steam and graphite,

especially in the reactor core with its high temperature level. The latter effect is included in the core model used in this analysis. Within the time interval considered, however, its influence on the pressure buildup is small and negligible with regard to the kinetics behavior of the core.

The amount of steam entering the primary circuit will be limited in this analysis in order to keep the pressure below the release pressure of the safety relief valves, which are provided for protection of the pressure vessel. A depressurization of the primary circuit caused by a release of these valves would result in a partial loss of the ingressed steam from the primary circuit. Thus, the effect of steam on the reactivity of the core is reduced and becomes insignificant for the subsequent neutron kinetics response. The plant will approach heat transfer conditions that do not differ essentially from those that would arise after a depressurization without steam ingress. An analysis of plant behavior under these conditions has been reported elsewhere[8] and, therefore, will not be discussed here. Graphite corrosion caused by steam remaining in the primary circuit can arise as an additional effect. This, however, is the result of insufficient heat removal from the core over an extended time interval so that the core temperature is kept at a sufficiently high level to support chemical reactions.

A termination of the steam ingress is achieved by interrupting the feedwater supply and by isolation of the steam generator from the primary circuit by switching off the gas blowers and closing the associated slide valves. With the normal shutoff procedure, the secondary feedwater supply is also interrupted. The transient behavior of the plant after termination of the water ingress essentially depends on the specific function of the protection system. It has not been investigated by detailed modeling because no additional aspects relevant to the short-term function of the shutdown system are expected from this period of time.

The rupture of a steam generator tube will cause a rapid transient of the two-phase flow inside this tube. The assumed stepwise pressure drop at the open end from its high initial value down to the comparatively low pressure of the primary circuit causes an initial ejection of steam at fairly high rates. If the feedwater supply continues at its initial value, however, the outlet flow rate, after passing through a maximum, will approach an asymptotic value determined by the feedwater supply rate.

The time dependence of the steam ingress rate and the associated steam enthalpy influences the initial rate of change of the core power. Therefore, it has been simulated by means of a dynamic steam generator program (SIKAN-E), which will be described in more detail in Sec. III.B.

The relationship between the steam ingress rate and the steam partial pressure at the inlet of the reactor core is not simple. The primary circuit can be regarded as a system of cavities that are connected by flow paths. The cavity containing the reactor core has a distributed heat source; the cavities containing heat removal components, such as the steam generator, act as heat sinks. The broken steam generator tube practically acts as a point source of mass and enthalpy.

Although it is assumed in the analysis that the gas blowers continue to circulate the helium steam mixture after initiation of the ingress, the steam distribution in the primary circuit deviates essentially from an even distribution as long as the inflow of steam persists. Time intervals of the order of 1 min are required after the termination of the ingress until a new state of equilibrium is obtained. The dynamic behavior of the primary circuit has been simulated in the present analysis with the COROX code, which will be explained in detail in Sec. III.A.

The SHOVAV-Jül reactor kinetics program, which will be described in detail in Sec. III.C, evaluates the instantaneous spatial distribution of the steam concentration inside the reactor core and the corresponding temperature distribution from the core inlet conditions. The steam inside the core is treated with regard to its neutron scattering and absorption properties as an additional materials core component, which has a time-dependent density and spatial distribution. The program evaluates the change of reactivity and the corresponding power transient from the disturbance of the neutron balance resulting from the appearance of steam in the core. The temperature dependence of reactivity is taken into account by the use of temperature-dependent neutron cross sections and by temperatures that are evaluated from a thermohydraulic model of the core.

Three computer codes, therefore, have been used in conjunction for simulating the systems response. The steam generator program provides the mass and enthalpy ingress boundary conditions to the COROX program. This code, in turn, provides the core inlet conditions for the reactor kinetics program, which evaluates the resulting core power transient. To include the feedback of the power generation in the core on the dynamics of the primary circuit, each calculation was repeated several times with updated core power until convergence of this iteration procedure was obtained.

The investigation of the rupture of a single tube resulted in an asymptotic ingress rate of 3.2 kg/s and showed a rather slow system response with insignificant reactivity effects. It was also decided, therefore, to perform a worst-case analysis, assuming the largest possible ingress rate from the steam generator irrespective of its probability. A water ingress was assumed, which results in an asymptotic ingress rate of 55 kg/s. This corresponds to the

simultaneous rupture of all parallel steam generator tubes. Thus, an upper limit for the consequences of possible ingress rates is obtained. Transients with arbitrarily chosen lower ingress rates and different values of the total ingressed mass have been analyzed in order to demonstrate the qualitative dependence of the systems response on these parameters.

III.A. The Primary Circuit Code COROX

The COROX program simulates the dynamic behavior of the primary circuit of an HTR. The following components of the primary system are included:

1. the reactor core, consisting of a packed bed of graphite spheres and the top and bottom reflectors of the core
2. the cold gas supply cavity at the core inlet and the heat collecting cavity at the core outlet
3. the different cavities containing heat exchanging equipment, such as steam generators and/or heat exchangers
4. the gas blowers used for circulation of the gas.

The circulating gas can be a mixture of different gas species with a composition that may vary with time. In the analysis presented in this paper, the gas mixture consists mainly of helium and water steam. Small amounts of hydrogen and carbon monoxide appear during the transient arising from graphite corrosion. For the analysis of water ingress accidents, the coolant is treated as a homogeneous mixture of helium and steam. The thermodynamic properties are evaluated from the usual correlations for gas mixtures.

The program is capable of treating the reactor core two-dimensionally in cylindrical geometry. For the present analysis, a one-dimensional option provided by the program has been used in order to be compatible with the one-dimensional treatment of the neutron kinetics by the SHOVAV-Jül code. This implies the tacit presupposition that the gas flow through the core can be described with sufficient accuracy as a parallel flow in the axial direction such that radial variations of flow velocities and gas temperatures can be replaced by averages that satisfy the overall energy balance.

The packed bed of the core is subdivided into a certain number of axial segments of equal height. The heat diffusion equation in a representative fuel sphere is solved for each segment under the assumption of spherical symmetry. The heat production inside the sphere is taken to be the spatial average of all spheres contained in the associated core segment. The heat production density is assumed to be constant within the inner fuel-graphite matrix and to be zero in the outer shell, which is free from fuel particles.

The gas flow through the core is modeled by two partial differential equations that represent the mass and energy balance of the gas flow in conservation law form in one spatial dimension. The energy equation is coupled via empirical heat transfer coefficients to the heat diffusion equation of the fuel spheres. Energy transport in the gas is assumed to be dominated by convection. Other transport mechanisms, such as heat diffusion in the gas and energy transport by absorption of radiation, are neglected. The system of coupled differential equations representing the reactor core is integrated by means of an implicit numerical algorithm.

The COROX code takes the top reflector and the core bottom into account because they form large heat storage capacities. The top reflector, therefore, may have an essential influence on the core inlet temperature if the gas temperature varies with time.

The top reflector and the core bottom structure consist of graphite blocks with a large number of parallel flow channels. They are treated in the program as media with heat diffusion and heat storage capacity coupled to the gas convection equation by heat transfer coefficients evaluated from empirical correlations valid for a pipe flow. The numerical treatment is analogous to that used for the packed bed of the core. The outlet temperature of the top reflector is transferred to the neutron kinetics program as a boundary condition for the core inlet temperature.

The mass inventory and temperature in the cavities of the primary system are evaluated from a mass and an enthalpy balance. For all cavities, complete mixing of all inlet flows and thermal equilibrium is assumed. This means that all outlet flows of a cavity have the same gas composition and the same temperature.

The average pressure in the primary system is evaluated from the total gas inventory and the gas temperatures in the different cavities, assuming that the gas mixture can be approximated as an ideal gas. This is an acceptable approximation as long as the partial pressure of steam is small compared with the total pressure. The deviations of pressures in the different cavities from the average pressure are small because frictional flow resistances are generally small. The frictional pressure drop across the reactor core, for instance, is ~0.2 bar for the initial flow rate.

Imposed boundary conditions, such as ingress mass and enthalpy rates and reactor power and steam generator outlet temperature, can be specified as time-dependent input functions.

III.B. The Steam Generator Program SIKAN-E

This program has been developed to simulate the transient behavior of a steam generator, which is heated by gas flow on the primary side. Cocurrent

and countercurrent flow with respect to the primary and secondary flow channels are admitted. The program is applicable to steam generators of the helix-bundle type. The secondary fluid flows through heat exchanging tubes that are arranged as bundles consisting of a large number of parallel tubes of equal length. All tubes are supplied by a common feeder pipe and are connected to a common riser so that a uniform pressure difference exists across each tube. The tubes are subject to cross flow of the primary gas. Parallel channel instability, therefore, is possible if heating of the different parallel tubes is not uniform. Under the operating conditions assumed in this analysis, however, perfect mixing in the primary gas flow and thus a uniform heating of all parallel tubes can be assumed. Since the evaporation process in one tube is representative of that in all parallel tubes, the primary flow can be treated as one-dimensional in space.

The secondary two-phase fluid is modeled by a system of coupled partial differential equations that represent the continuity, energy, and momentum equations for the liquid-steam mixture in conservation law form. An additional partial differential equation simulates the generation and recondensation of vapor bubbles in the subcooled boiling region. In the momentum equation inertia, friction and gravitational forces are taken into account. The equations are supplemented by empirical correlations for steam slip, two-phase friction, and for the incipience of nucleate boiling and film boiling. For the heat transfer between the two-phase fluid and the heat exchanging wall, different empirical heat transfer correlations are used that are appropriate to the local flow regime. The properties of water and steam as a function of local temperature and pressure are evaluated from analytic representations.

The primary fluid is described by an analogous set of differential equations, which is simpler because of the absence of phase changes. Heat transfer across the heat exchanging wall is simulated by the solution of the transient heat diffusion equation in one dimension, which is coupled via heat transfer coefficients to the secondary and primary fluids.

The system of differential equations is solved simultaneously by an implicit difference algorithm with second-order accuracy. Boundary conditions are satisfied by iterations.

III.C. Modeling of the Core Neutronics

The SHOVAV-Jül neutron kinetics program[9] has been used to simulate the neutron kinetics of the core in its mutual interdependence with the core thermohydrualics. This code is a modified version of the SHOVAV program,[10] originally developed for liquid-cooled reactors, made applicable to gas-cooled reactors with a pebble bed core. The code is a one-dimensional space-time kinetics program based on a multigroup diffusion approach. Up to four neutron energy groups and six groups of delayed neutrons can be taken into account.

Transients evaluated by this program always have to be started from a steady state as the initial condition. Several core parameters can be used to establish a steady-state solution of the system of difference equations underlying the program. In this analysis the initial state has been achieved by adjustment of the fission source strength.

The structure of the dynamic part of the SHOVAV-Jül code is shown in Fig. 4. A transient can be initiated by disturbing the neutron balance by modifying a boundary condition and/or the inner core composition. In the case of a water ingress, both types of disturbances actually become effective simultaneously. The coolant mass flow and the inlet temperature are time-dependent boundary conditions, and the steam content in the coolant modifies the inner core composition.

The spatial structure of the core is modeled by subdividing the core into a certain number of axial segments to which different materials compositions are assigned. In the present analysis, a subdivision of the core into nine equidistant segments has been used with nuclides compositions given in Table II. Two additional segments are used to represent the top and bottom core reflectors, which consist of fuel-free graphite. These materials segments are subdivided by

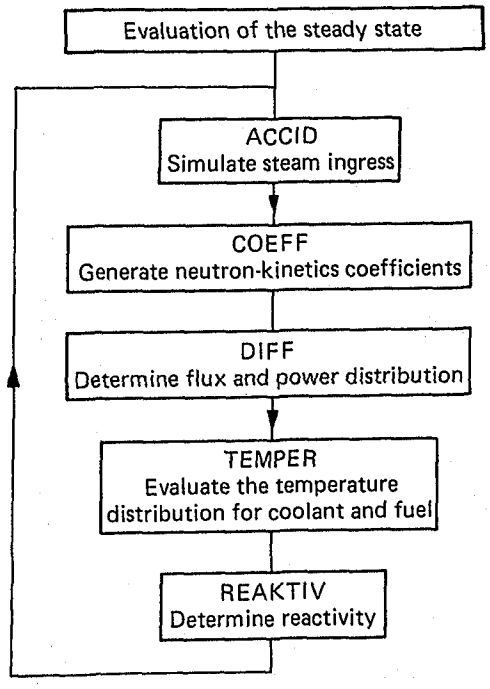

Fig. 4. Flow diagram for the dynamic part of the computer code SHOVAV-Jül.

TABLE II

Graphite and Main Heavy Metals in the Axial Core Segments

Core Region	Nuclide Concentrations (10^{24} atom/cm^3)						
	^{235}U	^{236}U	^{238}U	^{239}Pu	^{240}Pu	^{241}Pu	^{12}C
1	8.749E-6[a]	3.259E-7	9.813E-5	3.980E-7	6.635E-8	1.772E-8	5.129E-3
2	6.005E-6	8.099E-7	9.671E-5	7.057E-7	2.649E-7	1.222E-7	5.129E-3
3	3.950E-6	1.148E-6	9.516E-5	7.340E-7	3.975E-7	2.465E-7	5.129E-3
4	2.857E-6	1.309E-6	9.402E-5	6.847E-7	4.246E-7	3.007E-7	5.129E-3
5	2.285E-6	1.385E-6	9.329E-5	6.357E-7	4.257E-7	3.067E-7	5.129E-3
6	1.963E-6	1.424E-6	9.283E-5	5.962E-7	4.298E-7	2.972E-7	5.129E-3
7	1.778E-6	1.445E-6	9.254E-5	5.693E-7	4.279E-7	2.909E-7	5.129E-3
8	1.671E-6	1.456E-6	9.236E-5	5.522E-7	4.244E-7	2.8630E-7	5.129E-3
9	1.604E-6	1.463E-6	9.226E-5	5.356E-7	4.211E-7	2.822E-7	5.129E-3

[a]Read as 8.749×10^{-6}.

additional horizontal planes. Thus a fine mesh is generated that is used for the numerical solution of the system of neutron diffusion equations to calculate flux and power distribution. The nuclear design data of the core and of the fuel sphere are given in Table III.

The neutron cross sections for the core materials are required by the program as input values for the four energy groups. Two options exist for providing these data. Specifying microscopic cross sections for all nuclides that appear in the core is the first possibility. In this case macroscopic cross sections for every materials segment will be generated by the program from the specified materials compositions. Alternatively, macroscopic cross sections that have been generated by another program can be specified by input for every materials segment. The choice between the two options is a question of computing economy. In the present case, where ~50 different nuclides with spatially varying compositions appear in the core, the second option has been applied. The core composition underlying the present analysis is that of a core with an average burnup of 10^5 MWd/ton. The cross-section data set was generated by an auxiliary program (MUPO), to which we shall refer again later in this paper.

The temperature dependence of the cross sections can be taken into account by generating cross-section data sets at different temperatures. The values of a certain cross section at different temperatures will be used as supporting points of a polygonal representation of the temperature dependence of the cross section. In the case of simulating a transient, SHOVAV-Jül will use these functions to evaluate instantaneous local cross sections according to the instantaneous local fuel and moderator temperatures. For this analysis, six data sets have been generated for six equally spaced temperatures in the range from 300 to 1400°C.

The simulation of the temperature feedback on reactivity differs in principle from a commonly used approach, which is based on some scalar temperature coefficient of reactivity related to the average temperature of the core or to some other reference temperature. This type of approach would not be

TABLE III

Nuclear Design Data of the Core and Fuel Spheres

Core dimensions	
Radius, cm	280
Height, cm	507.5
Reflector thickness	
Top, cm	200
Bottom, cm	100
Side, cm	130
Enrichment zones	
Number	2
Outer radii, cm	196/280
Loading scheme	OTTO
Fuel sphere	
Total radius, cm	3.0
Radius of the fuel matrix, cm	2.5
Fuel material	UO_2
Heavy metal content per sphere, g	8
Coated fuel particle	
Density of kernels, g/cm^3	10.9
Thickness of coatings, μm	90/40/35/35
Density of coatings, g/cm^3	0.9/1.85/3.2/1.85
Average burnup, MWd/ton	100.000
^{235}U enrichment, inner/outer, %	6.8/12.6

able to account for changes of the temperature distribution inside the core during a transient.

Core temperatures, in turn, are evaluated simultaneously with the neutron kinetics from a thermohydraulic model of the core, which is part of the SHOVAV-Jül code. This model corresponds to the one-dimensional version of the thermohydraulics core program, which is integrated into the COROX code (described in Sec. III.A). However, in addition to the graphite temperature of the fuel spheres, the SHOVAV-Jül version also calculates the temperature of the fuel kernels inside the coated particles. This kernel temperature is interpreted by the neutron kinetics part of the code as fuel temperature; whereas, the average temperature of the graphite matrix and of the outer graphite shell of the fuel spheres is taken as the moderator temperature. With high-power generation, the fuel temperature may be significantly higher than the temperature of the surrounding matrix graphite due to the heat resistance of the surrounding graphite coating and to the finite thermal conductivity of the kernel. The temperature difference between kernel and matrix graphite is calculated from a steady-state heat diffusion equation for a representative fuel particle in each fuel sphere.

The local steam concentration inside the core is calculated from the equation of state for an ideal gas. The steam partial pressure is approximated as being spatially constant within the core, and the gas temperature is provided by the solution of the energy equation for the gas flow. The axial variation of the gas temperature therefore results in an axial variation of the gas and steam density. It is further assumed that the mixture of helium and steam that enters the core is homogeneous and, therefore, has no radial variation of the steam density inside the core. The change of the local macroscopic cross section inside the core, caused by the addition of steam, is evaluated from the microscopic cross sections of water and the steam molecular concentration for the local gas temperature.

The neutron cross section of the core materials was generated by condensing multigroup data sets to four energy groups. For this purpose, the neutron spectral MUPO program[11] was used. A zero-dimensional multigroup diffusion program, MUPO has a cross-section library for 43 energy groups. Neutron leakage can be approximately taken into account by input specification of energy dependent buckling values. Neutron spectra are obtained from a steady-state solution of the system of multigroup diffusion equations where the steady-state condition is achieved by iterative adjustment of k_{eff}. These spectra are then used to condense the 43 energy groups to the 4 groups required by the SHOVAV-Jül code.

The microscopic neutron cross sections for water contained in the data library of the MUPO code have also been condensed to four energy groups using the neutron spectrum generated by the same code. Figure 5 shows the total microscopic cross section of water as a function of energy together with this neutron spectrum. It is that of the materials segments in the upper part of the core, which has the highest weight with regard to reactivity for a fuel temperature of 910°C and a moderator temperature of 865°C. The change of the neutron spectrum due to the presence of steam in the different core segments has been neglected since the contribution of the steam to the macroscopic cross sections is small throughout the core. The steam molecular density, which is used to generate the macroscopic cross sections of water, is calculated as a time-dependent function in the course of a transient.

The fission power generation is evaluated from the system of transient diffusion equations for the four groups of neutron fluxes and an additional system of equations representing the generation and the decay of delayed neutrons.

Six delayed neutron groups are taken into account, emerging from the fissile nuclides ^{235}U, ^{239}Pu, and ^{241}Pu. The abundances and decay constants for the delayed neutrons used were taken from Ref. 12. Since the concentration of the different fissile nuclides is space dependent inside the core, a set of six equations for the delayed neutrons is attributed to each materials segment of the core with the appropriate delayed neutrons source strength resulting from the local concentration of the different fissile nuclides. Since the decay constants of the delayed neutrons are nearly the same for the three source nuclides, average decay constants λ_m are used for every group, which are calculated from

$$\frac{1}{\lambda_m} = \sum_n (\beta_{mn}/\lambda_{mn}) \Big/ \sum_n \beta_{mn} \ ,$$

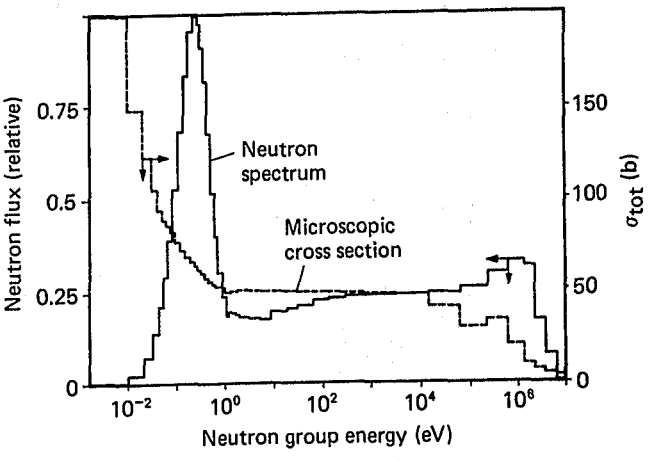

Fig. 5. Neutron spectrum at the upper part of the core and the total microscopic cross section of water as a function of energy.

where

β_{mn} = abundance of the m'th delayed neutron group generated from the n'th fissile nuclide

λ_{mn} = associated decay constant.

Since the reactivity does not appear explicitly in the time-dependent diffusion equations, there is an option for evaluating the instantaneous reactivity from a perturbation approach.

IV. RESULTS

IV.A. Water Ingress Rates

Figure 6 shows a greatly simplified schematic of the steam generator that may serve to assist understanding of the following considerations. The helical tube bundles of the steam generator are represented by several straight tubes, which form parallel flow paths to a broken tube between a common feeder and a common riser plenum.

The pressure difference between the feeder and the riser in the initial state is mainly determined by the flow resistance of the tubes. If only one tube fails, or even a small number compared with the total of 168 tubes, and if the feedwater supply is maintained constant, then this pressure difference will not be essentially changed. The gas temperature profile along the tubes will also remain practically unchanged because the surface of the broken tube only represents a small contribution to the total heat exchanging area.

The total ingress rate is the sum of the exit flow rates from both parts of the broken tube. In the following we shall denote the part of the broken tube between the rupture location and the feedwater supply as the "cold leg" and the other part as the "hot leg" of the tube.

In case of a single tube failure, these two flow rates have been evaluated by the SIKAN-E program with the following assumptions. The pressure in the common feeder and in the common riser volume is kept constant at its initial value throughout the transient. The same is assumed for the inlet temperature, which is the feedwater temperature in the case of the cold leg and the temperature of the superheated steam from the intact tubes in the riser volume in the case of the hot leg.

The tube rupture is simulated by a stepwise drop of the secondary pressure at the anticipated location of the rupture from its initial 125-bar value to the pressure of the primary system (40 bar).

Immediately after the rupture, a sharp increase of the exit flow rate is observed, which, for a short period of time, is limited by the critical flow rate (~1.15 kg/s). The exit flow rate passes through a maximum and decreases; whereas, an expansion wave travels through the tube from the outlet to the inlet. After ~0.5 s, the exit flow passes through a minimum and increases then to approach a new steady-state value of 2.3 kg/s. In Fig. 7, the difference between the outflow and feedwater inflow indicates that

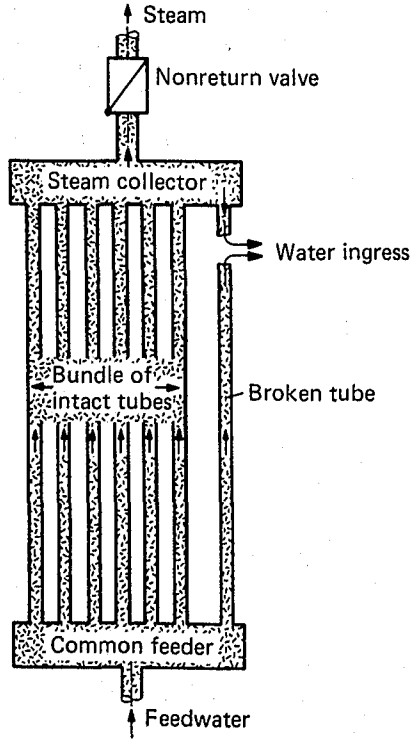

Fig. 6. A simplified schematic of the steam generator with a tube rupture.

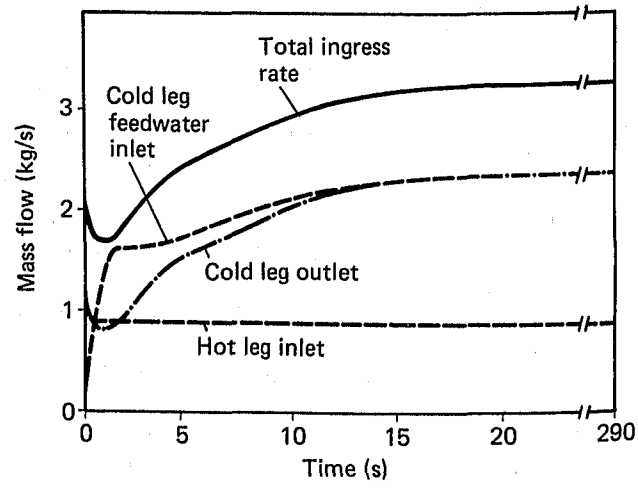

Fig. 7. Mass flow rate resulting from the rupture of one steam generator tube.

nonequilibrium conditions prevail inside the broken tube over a time interval of ~15 s.

The fluid outlet temperature of the cold leg drops rapidly from its initial value of 550°C and attains the saturation temperature corresponding to the pressure of the primary circuit ~2 s after the rupture. A two-phase flow emerges from the broken tube in the following time interval with the steam quality approaching an asymptotic value of 12%. This effect results from a shift of the evaporation region inside the tube toward the outlet opening.

In the hot leg of the broken tube, this time interval is much smaller. Equilibrium conditions are attained within <1 s. The exit flow of this tube rapidly attains a steady-state value of 0.9 kg/s. The outlet temperature approaches a steady-state value of 475°C.

The effective ingress temperature shown in Fig. 8 is calculated from an enthalpy obtained from a mass-flow-weighted average of the two contributions to the total ingress rate. It can be regarded as a representative temperature for the total ingress rate if it is assumed that the two ingress flows will be perfectly mixed at their exit and that thermal equilibrium is immediately established.

The assumptions that have been made for the rupture of one tube are also applicable to the simultaneous rupture of more than one tube if the number of broken tubes remains small compared with the total number of parallel tubes in the bundle. Total ingress rates under these conditions are simply obtained by multiplying the rates evaluated for one tube with the number of broken tubes.

A different situation exists if a simultaneous rupture of all tubes is assumed. In this case the behavior of one tube is representative of all tubes, but the temperature profile of the primary gas flow will experience a transient due to the heat transfer change between the primary and secondary fluids. In this case the cold leg of the tubes will provide the main contribution to the ingressed mass because of the continuous supply of feedwater. The contribution of the hot leg remains small because the riser plenum is separated from any mass supply and therefore undergoes a depressurization, which is achieved by the loss of a relatively small amount of steam contained in that part of the circuit which comprises the riser volume up to the point where a provided check valve will interrupt the backflow of steam.

The simulation of the cold leg with the feedwater supply and the inlet temperature kept constant yields results that are shown in Figs. 9 and 10. The flow rate

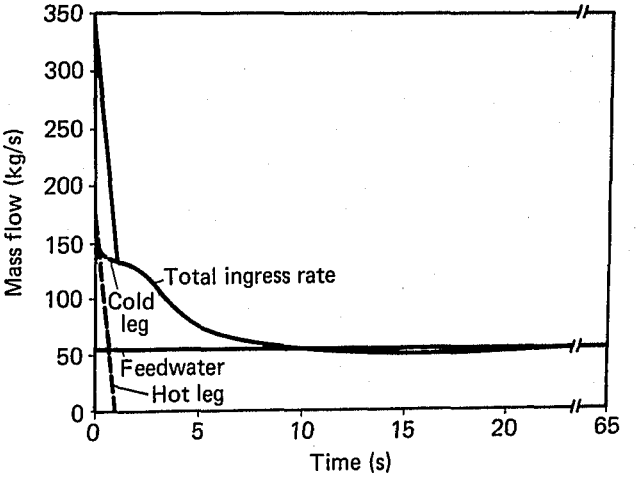

Fig. 9. Mass flow rate resulting from the rupture of all steam generator tubes.

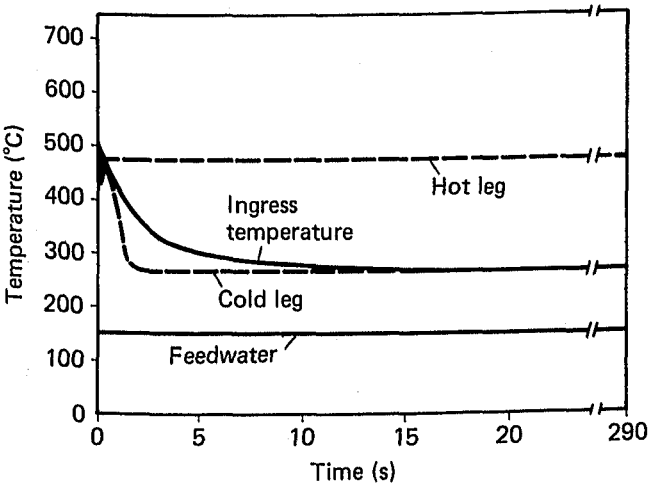

Fig. 8. Secondary fluid temperatures resulting from the rupture of one steam generator tube.

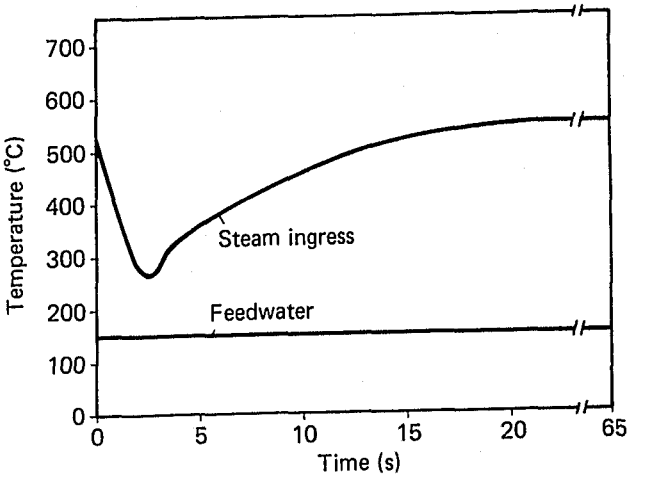

Fig. 10. Secondary fluid temperatures resulting from the rupture of all steam generator tubes.

again shows an initial maximum limited by the critical flow rate, which, in this case, amounts to ~350 kg/s. The maximum flow rate is followed by a monotonous decrease. Nearly steady-state conditions are attained within ~10 s. The steady-state exit flow (being equal to the feedwater supply rate) is 55 kg/s. Within the first 3 s, the steam outlet temperature decreases from 550°C to the corresponding saturation temperature of the primary circuit pressure (250°C). This temperature drop results from a spread of the evaporation region inside the tube. An increase of the outlet temperature is predicted in the ensuing time period that approaches a steady-state value of 545°C, which is almost attained in ~15 s.

The depressurization of the hot leg is a rapid process, which yields a significant mass flow contribution only over a short time interval of ~1 s.

IV.B. Pressure and Temperature Transients in the Primary System

The response of the primary system to the mass and enthalpy ingress from the defective steam generator as predicted by the COROX code is shown in Figs. 11 through 17. A constant volume flow of the gas blowers is assumed in all cases. The figures display the pressure buildup, the gas temperature and the steam partial pressure at the core inlet, and the core mass flow as a function of time. Figures 11, 12, and 13 are related to an ingress with an asymptotic rate of ~7 kg/s, which corresponds to the simultaneous rupture of two steam generator tubes; whereas, Figs. 14 through 17 represent the case of an ingress with an asymptotic rate of 55 kg/s, which corresponds to the simultaneous rupture of all tubes. The total ingressed mass is limited to 2 tons of water. In the latter case, results for a total ingressed mass of 4 tons are also shown.

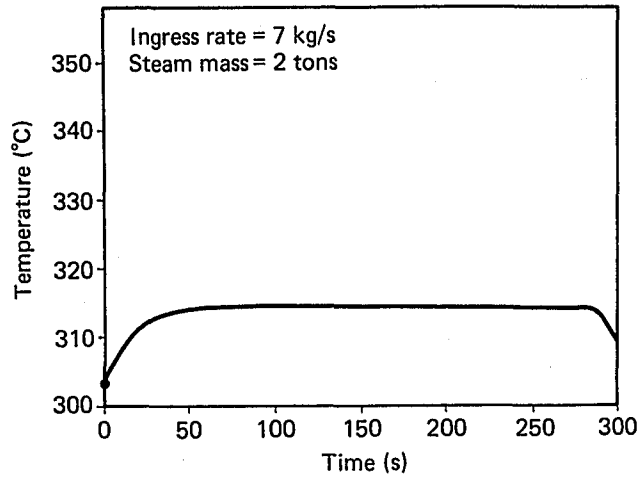

Fig. 12. Temperature transient in the cold gas plenum with low ingress rate (7 kg/s).

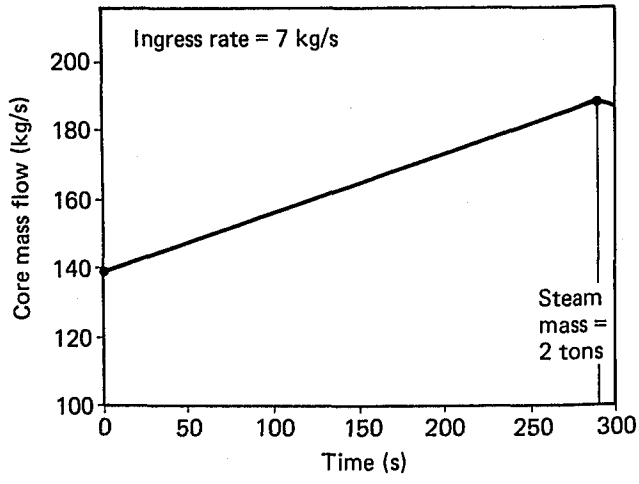

Fig. 13. Increase of the mass flow in the core during the water ingress with low ingress rate (7 kg/s).

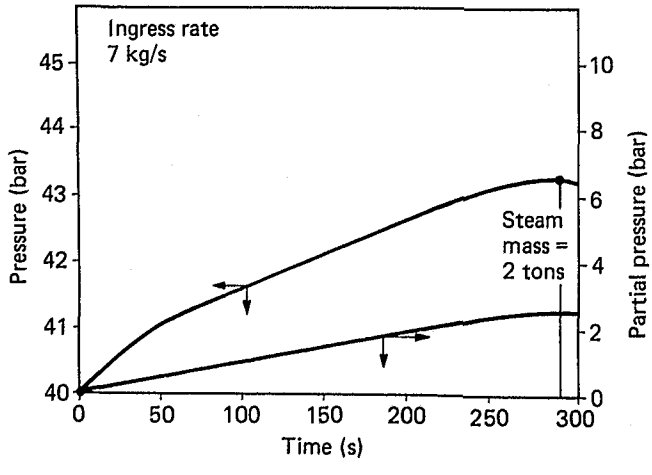

Fig. 11. Pressure transients in the primary system during a water ingress accident with low ingress rate (7 kg/s).

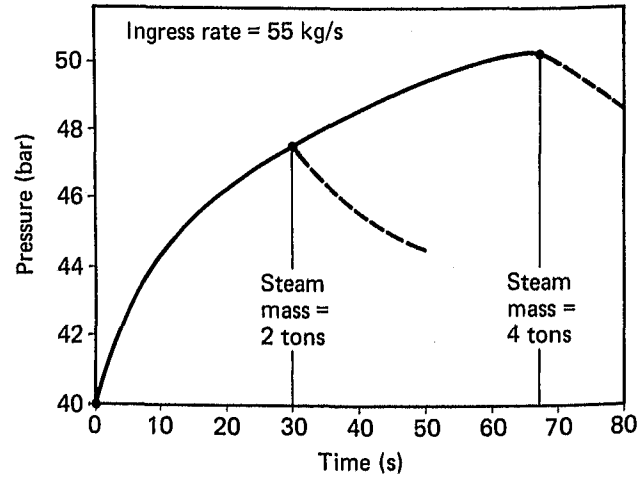

Fig. 14. Pressure transients in the primary system during a water ingress accident with high ingress rate (55 kg/s).

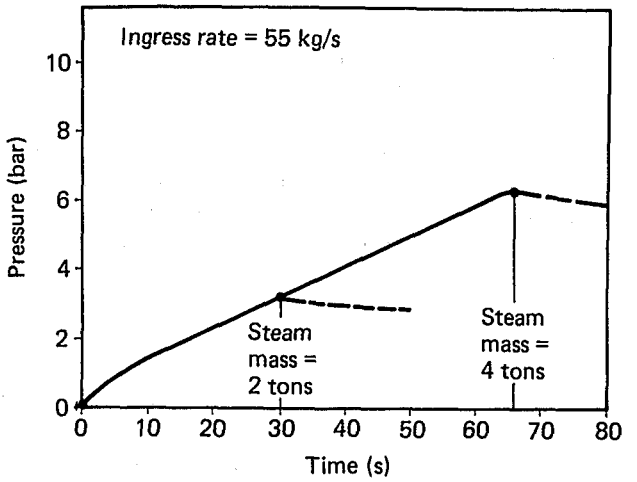

Fig. 15. Steam partial pressure in the cold gas plenum with high ingress rate (55 kg/s).

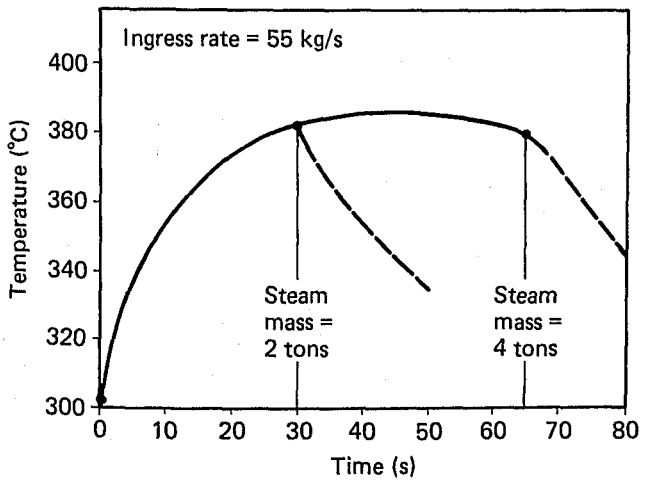

Fig. 16. Temperature transients in the cold gas plenum with high ingress rate (55 kg/s).

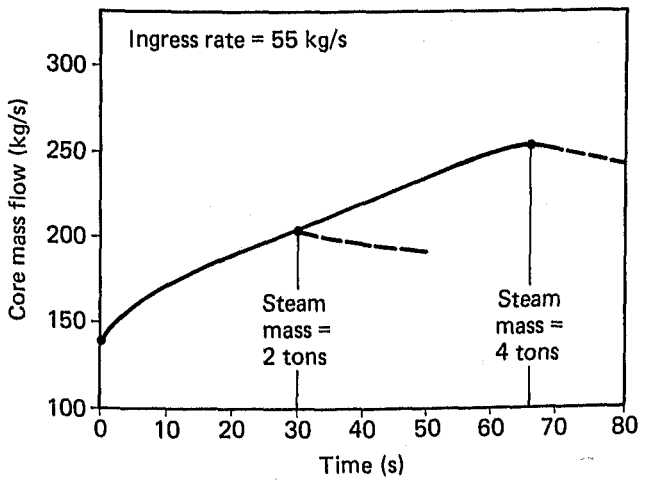

Fig. 17. Increase of the mass flow in the core during the water ingress with high ingress rate (55 kg/s).

Figures 11 and 14 show the pressure increase in the primary system during the ingress period. After termination of the ingress, a slight decrease of pressure is observed for a period of ~10 s resulting from a decrease of the gas temperature in the primary system. This temperature drop occurring after the interruption of the ingress, however, can only be expected to persist for a rather short period of time. It is caused by some heat removal via the defective steam generator, which is kept effective by the blower during its running-down period. Finally, the heat removal by the steam generator is nearly stopped by the closing slide valves, which isolate the steam generator from the primary system. The development of conditions in the primary system during the subsequent period of time is determined by the manner in which the plant protection system will again take up the heat removal by the auxiliary system.

The core mass flow is the product of the gas density at the blower inlet and the volume flow rate. Since the volume flow is assumed to be constant, the mass flow as shown in Figs. 13 and 17 actually represents the time dependence of the density of the gas/steam mixture. Since the power consumption of the blowers increases with increasing mass flow and since the blower control tends to keep the volume flow rate constant, an unexpected increase of power demand by the blowers could serve as an additional indication of a failure in the steam generator.

Whereas the rupture of a few tubes produces rather slow transients as shown in Figs. 11, 12, and 13, the rupture of all tubes could result in a pressure increase that will exceed the design pressure after ~1 min (Fig. 14). The total mass of steam ingress up to this time is ~4 tons. The gas temperature in the cold gas plenum increases from 303 to ~385°C and thus slightly surpasses the design temperature (380°C). This occurs after ~30 s of ingress. With termination of the ingress, however, the temperature again falls below the design value.

The graphite corrosion due to a chemical reaction of the steam with the graphite in the core remains very small within the time interval of several minutes being investigated. The gaseous products of the corrosive reaction (carbon monoxide and hydrogen) only yield a very small contribution to the total pressure buildup.

IV.C. Reactivity and Power Transients

The neutron kinetics response of the system for the large ingress rate just considered is shown in Fig. 18. The reactivity experiences a relatively fast initial increase, passes through a maximum at ~8 s, and decreases rapidly in the succeeding time period. After ~30 s, however, the positive reactivity passes

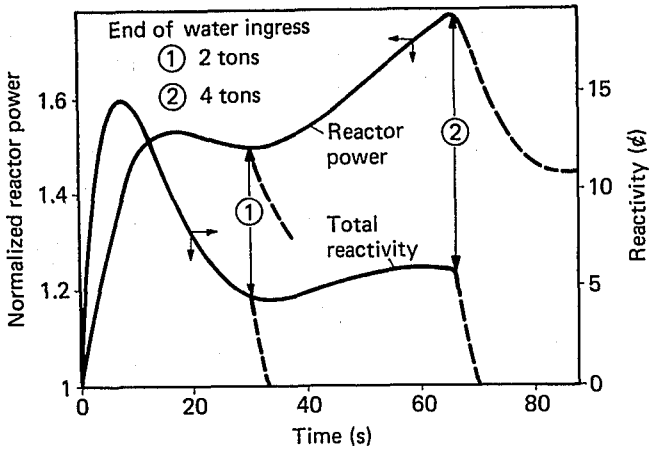

Fig. 18. Reactivity and power transients resulting from a water ingress accident with a rate of 55 kg/s.

through a minimum and moderately increases until the end of the ingress.

This behavior is a consequence of the counteraction of steam and temperature effects on reactivity. The reactivity increases if the rate of reactivity gain by the increasing steam concentration inside the core is larger than the rate of reactivity loss caused by an increasing core temperature and vice versa. In the initial period of time, the steam effect is dominant because the core temperature follows the power increase with some delay. With increasing time, however, the negative temperature effect on reactivity grows to an extent that the steam effect is exceeded. During this period the reactivity passes through the first maximum, which is followed by an intermediate reactivity drop. The reactor power shows a qualitatively similar behavior with a slight decrease after the first power maximum within a time interval of ~20 s. This results from the sharp decrease of reactivity after passing through the maximum and is mainly due to the time behavior of the delayed neutrons with short lifetimes. In the subsequent period, however, the temperature effect loses some of its effectiveness so that after 30 s the reactivity gain by the increasing steam concentration becomes slightly larger than the reactivity loss from the temperature increase.

The alternating effectiveness of the core temperature is a consequence of the transient energy balance in the core, which is characterized by a large heat storage capacity. In the first period of time up to ~30 s, fuel temperatures show increased rates of growth. This results not only from the increasing heat generation, but also from an enhanced storage of heat in the fuel spheres because increasing gas inlet temperatures counteract the heat flow to the gas during this period of time. The augmented heat storage results in a temperature rise inside the fuel spheres, which is larger than what would be expected from the instantaneous power generation only. The increase of reactivity observed after ~30 s results from a reduced temperature effect on reactivity, which stems from a reduced rate of temperature increase inside the spheres due to decreasing power generation and a growing heat flow from the fuel spheres to the coolant during this stage. The temperature effects described are effective only within the upper 2 m of core height. In the lower part of the core, the heat flow rate to the coolant remains practically constant.

The analysis of this worst case shows that no serious consequences for the core are to be expected. The first maximum of the reactivity attains a value of 15.0¢. The final reactivity at the end of the ingress amounts to 6.0¢. The power is leveled off at ~155% of the initial power within the first 35 s. Finally it increases to ~180% at the end of the ingress. The maximum power gradient during the accident is ~25 MW/s.

After termination of the ingress and isolation of the defective steam generator, a decrease of reactivity and reactor power is observed. Figure 18 shows that this effect is qualitatively independent at the instant of termination. It results from a core temperature rise, which persists some time after termination of the ingress due to the loss of the steam generator as a heat sink.

Figure 19 shows the time dependence of the average temperature in fuel spheres at different axial positions of the core. Figures 20 and 21 display the axial distribution of the coolant and sphere average temperature at several selected time levels. The figures show that significant rates of change are restricted to the upper part of the core where the power density is much greater than the lower part.

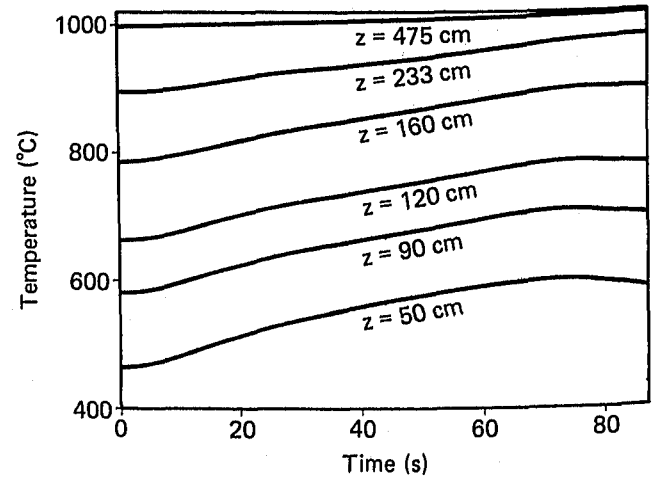

Fig. 19. Transients of the average temperature of the fuel spheres at different core positions.

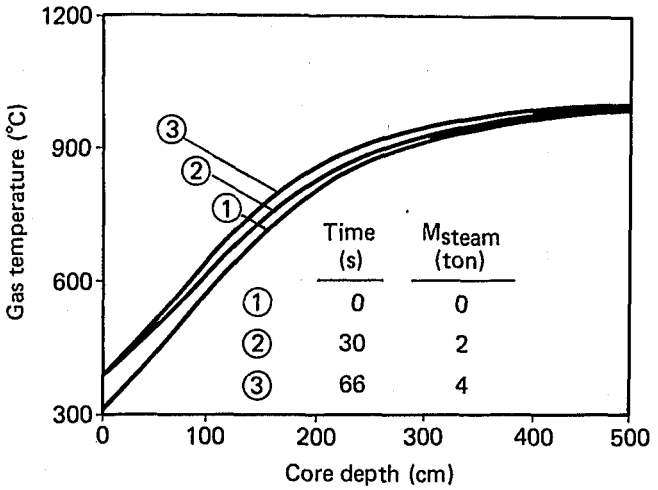

Fig. 20. Axial distribution of the coolant temperature at selected time levels.

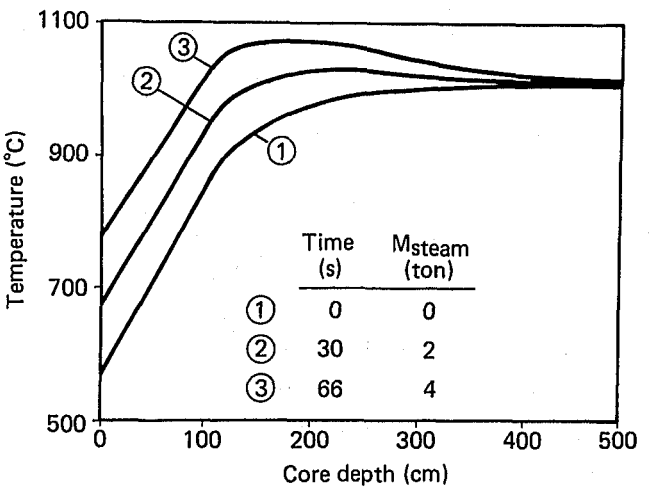

Fig. 22. Axial distribution of the temperature of the fuel kernels in the center of the spheres at selected time levels.

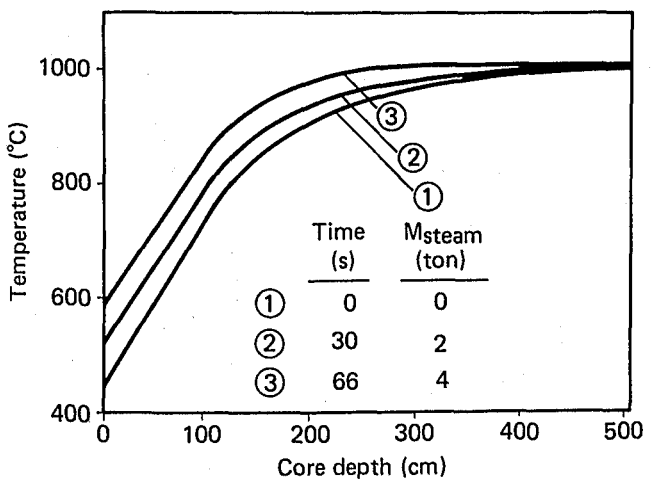

Fig. 21. Axial distribution of the sphere average temperature at selected time levels.

Since the coolant outlet temperature is rather insensitive to the ingress rate, it could not be used as an indication of the accident within 1 min.

At the assumed termination of the ingress (at t = 66 s), average temperatures of the fuel spheres in the inlet plane of the core attain values that are up to 135°C higher than the values at nominal power. This is a consequence of the increasing power and of the increasing gas inlet temperature as shown in Fig. 16.

Figure 22 shows the axial distribution of the temperature of the fuel kernels in the center of the spheres for several time levels including the initial state. The maximum fuel temperature attained at the instant of termination of ingress is 1075°C. This corresponds to an increase of 120°C against the initial value. The highest rate of temperature change in the fuel kernels is ~2.8°C/s. Kernel temperatures and heatup rates remain below the limit at which damage to the coating of the fuel particles can be expected.

The results for an asymptotic ingress rate of 7 kg/s, corresponding to the rupture of two steam generator tubes, are shown in Figs. 23 through 26. The termination of ingress is assumed at 290 s where 2 tons of steam have entered the primary system.

The time dependence of the reactivity and the reactor power for this case are shown in Fig. 23. A small increase of reactivity is observed in this case, too, but a pronounced maximum of the reactivity like that in the case considered before does not come about. After the initial increase, the reactivity remains practically constant at a value of ~1.2¢ causing

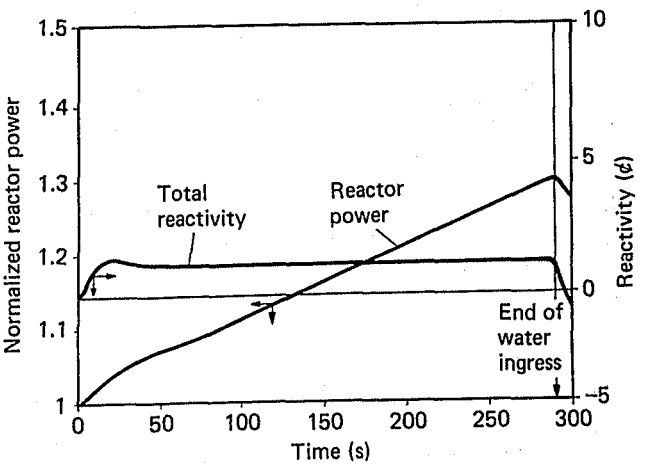

Fig. 23. Reactivity and power transients resulting from a water ingress accident with a rate of ~7 kg/s.

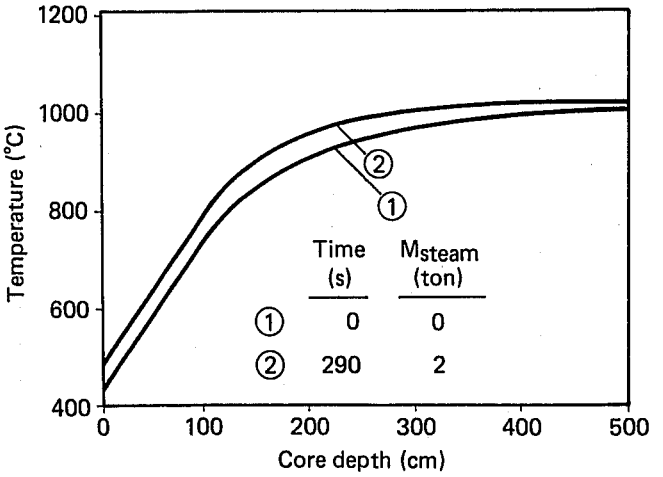

Fig. 24. Axial distribution of the sphere average temperature at the termination time of steam ingress including the initial state.

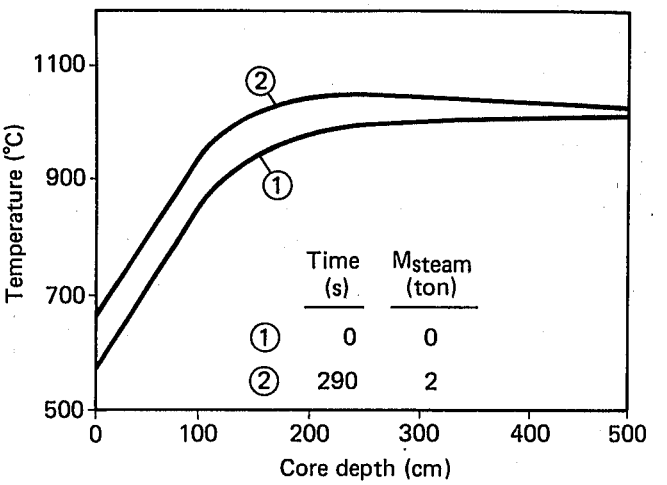

Fig. 26. Axial distribution of the fuel kernels in the center of the sphere at the termination time of steam ingress including the initial state.

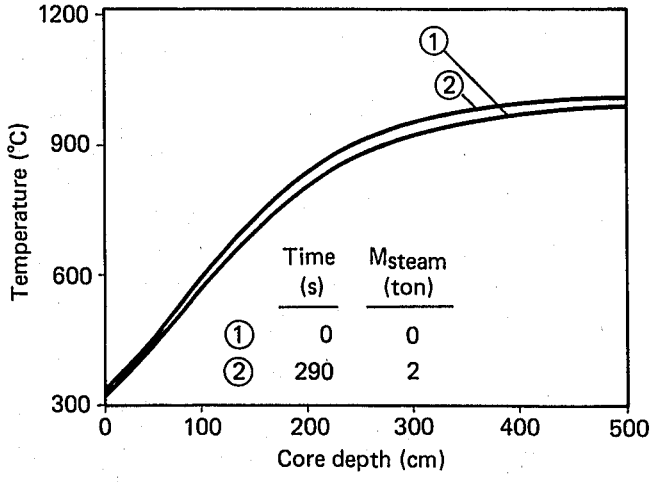

Fig. 25. Axial distribution of the coolant temperature at the termination time of steam ingress including the initial state.

a slow, nearly linear increase of reactor power. At the instant of ingress termination, it attains a value of 130% of the initial power. After termination of the ingress, a decrease of power and reactivity is observed for the same reason as in the example previously discussed.

The axial distribution of temperatures shown in Figs. 24, 25, and 26 exhibits the same qualitative behavior but with correspondingly lower rates of change. The maximum reactor power gradient during the accident is ~5 MW/s. The maximum temperature increase of the fuel kernels in the center of the spheres in this case amounts to only 85°C.

V. CONCLUSIONS

The presented analysis shows that, because of the inherent safety features of the high-temperature gas-cooled reactor, the consequences of even a worst-case water ingress accident are limited. For the highest ingress rate of 55 kg/s and for 4 tons of water in the primary circuit, the power level of 180% is reached. The maximum fuel temperature remains <1100°C. For the evaluated 2.8°C/s increase rate of the fuel temperature, a failure of the coated particles is not to be expected. The results of the space-time kinetic analyses show that no special requirements on the promptness of control rod actions are needed to limit the accident consequences in the core. Due to the increasing pressure and mass flow over an extended time range, counteractions are nevertheless required to limit the system pressure and to avoid superheating of the heat removal system. Several protective devices are available for the sufficiently early recognition of a water ingress accident.

In the case of the high ingress rate, the primary system pressure is the first critical plant condition attained when no previous counteraction becomes effective. The time available for a protective action is at most the time that elapses until the design value of the pressure is approached. In the worst case, however, this time span is in the range of ~1 min.

Within this time range, several automatic protective actions will be activated on recognizing the water ingress accident and counteractions will be initiated. These are mainly the response thresholds for the reactor power, neutron flux gradient, the moisture, and pressure values. Our results show for example that the typical limits for the nuclear power (110%) and for the power gradient (10 MW/s) are exceeded

within the first 2 s, whereby the reactor shutdown is initiated. Moreover, the pressure scram at ~42 bar will be reached after 5 s. The next safety signal will be produced by the moisture surveillance system after ~10 s. In addition, the increase of electrical power to the blower provides another safety signal to detect the defective loop and to interrupt the accident.

In the case of the low ingress rate, a rather slow increase of power and core temperature will result. The design value of the pressure would be exceeded not earlier than several minutes after initiation of the ingress. The response threshold to the moisture and pressure values will be reached after 10 s and 2 min, respectively. In this case, the maximum gradient of the reactor power is expected to be much smaller than the scram limit, which is usually used by the protection system. The shutdown limit, which will afterwards be exceeded, is the high-power scram level after 90 s. This, however, is to be expected only if the automatic power control system is inoperative. The rate of reactivity change is small enough in this case that a properly working control system with adjusting absorber rods would be able to compensate for the gain of reactivity caused by the steam ingress.

REFERENCES

1. V. DRÜKE, D. FILGES, N. KIRCH, and R. D. NEEF, "Experimental and Theoretical Studies of Criticality Safety by Ingress of Water in Systems with Pebble-Bed High-Temperature Gas-Cooled Reactor Fuel," *Nucl. Sci. Eng.*, **57**, 328 (1975).

2. V. F. SCHÜRRER and R. D. NEEF, "Reaktorphysikalische Auslegung kritischer Experimente am Siemens-Argonaut-Reaktor Graz zum Studium des Wassereinbruchs in Schüttungen kugelförmiger Brennelemente," *Atomkernenergie-Kerntechnik*, **37** (1981).

3. H. J. SCHARF, "Untersuchungen zur Kurzzeitdynamik von OTTO-Kugelhaufenreaktoren," Jül-1169, Kernforschungsanlage Jülich (Feb. 1975).

4. K. SCHULTES, "Untersuchungen zum Temperaturkoeffizienten und zur Kurzzeitdynamik am Kugelhaufen-Hochtemperaturreaktor PNP-3000," Jül-1566, Kernforschungsanlage Jülich (Jan. 1979).

5. H. ENGELBRECHT, "Analysen zur Dynamik von Kugelhaufen-Hochtemperaturreaktoren," Jül-Spez-123, Kernforschungsanlage Jülich (Aug. 1981).

6. R. NABBI, G. MEISTER, W. JAHN, and W. REHM, "Sicherheitsanalysen zur Neutronenkinetik eines Kugelhaufen HTR-Cores bei hypothetischen Wassereinbruchstörfallen," *Jahrestagung Kerntechnik*, Düsseldorf (Mar. 1981).

7. Bergbau-Forschung GmbH, GHT Gesellschaft für Hochtemperaturtechnik mbH, Hochtemperatur-Reaktorbau GmbH, Kernforschungsanlage Jülich GmbH, Rheinische Braunkohlenwerke AG, "Referenzkonzept der Prototypanlage Nukleare Prozesswärme Band 1: Gesamtanlage und Kraftwerk," GHT-Ident-Nr. 78.02633 (Sep. 1981).

8. J. A. FASSBENDER, W. KATSCHER, W. REHM, and J. P. WOLTERS, "State of HTGR Safety and Future Developments," *Proc. Conf. Gas Cooled Reactors Today*, Bristol, September 20-24, 1982, British Nuclear Energy Society, **3**, 7 (Sep. 1982).

9. R. NABBI, G. MEISTER, R. FINKEN, and M. HABEN, "SHOVAV-Jül: Ein eindimensionales Neutronenkinetik-Programm für Kugelhaufen-Hochtemperaturreaktoren mit Temperatur- und Xenon-Rückkopplung," Jül-Spez-171, Kernforschungsanlage Jülich (Sep. 1982).

10. D. SAPHIER and S. YIFTAH, "SHOVAV—A Program to Solve the Few-Group Space-Time Dependent Diffusion Equation with Temperature Feedback," IA-1217, Israel Atomic Energy Commission (Jan. 1977).

11. J. SCHLÖSSER, "MUPO, An IBM-7090 Programme to Calculate Neutron Spectra and Multi Group Constants," Dragon Report 172, Atomic Energy Establishment, Winfrith (1963).

12. L. TOMLINSON, "Delayed Neutron from Fission, A Compilation and Evaluation of Experimental Data," AERE-R 6993, Atomic Energy Research Establishment, Harwell (1972).